AIP | Physics of Plasmas

The absorption mechanisms of whistler waves in cool, dense, cylindrically bounded plasmas

B. M. Harvey and C. N. LashmoreDavies

Citation: Phys. Fluids B **5**, 3864 (1993); doi: 10.1063/1.860609
View online: http://dx.doi.org/10.1063/1.860609
View Table of Contents: http://pop.aip.org/resource/1/PFBPEI/v5/i11
Published by the American Institute of Physics.

Related Articles

Time growth rate and field profiles of hybrid modes excited by a relativistic elliptical electron beam in an elliptical metallic waveguide with dielectric rod
Phys. Plasmas 19, 102110 (2012)

Toroidal rotation of multiple species of ions in tokamak plasma driven by lower-hybrid-waves
Phys. Plasmas 19, 102505 (2012)

Wave breaking phenomenon of lower-hybrid oscillations induced by a background inhomogeneous magnetic field
Phys. Plasmas 19, 102302 (2012)

Measurements of ion cyclotron range of frequencies mode converted wave intensity with phase contrast imaging in Alcator C-Mod and comparison with full-wave simulations
Phys. Plasmas 19, 082508 (2012)

Backward mode of the ion-cyclotron wave in a semi-bounded magnetized Lorentzian plasma
Phys. Plasmas 19, 082101 (2012)

Additional information on Phys. Fluids B

Journal Homepage: http://pop.aip.org/
Journal Information: http://pop.aip.org/about/about_the_journal
Top downloads: http://pop.aip.org/features/most_downloaded
Information for Authors: http://pop.aip.org/authors

ADVERTISEMENT

Downloaded 08 Nov 2012 to 194.81.223.66. Redistribution subject to AIP license or copyright; see http://pop.aip.org/about/rights_and_permissions

The absorption mechanisms of whistler waves in cool, dense, cylindrically bounded plasmas

B. M. Harvey and C. N. Lashmore-Davies
AEA Technology, Fusion, Culham Laboratory (Euratom/UKAEA Fusion Association), Abingdon, Oxon OX14 3DB, England

(Received 1 June 1993; accepted 20 July 1993)

It can be shown that whistler waves with low parallel phase velocity can be subject to strong cyclotron damping, even when the wave frequency is well below the cyclotron frequency. This resonance arises as a result of the Doppler effect which is proportional to the plasma density and increases the frequency experienced by electrons moving in the opposite direction to the wave. In this paper the dispersion relation of whistler waves in a cylindrically bounded plasma is obtained and then solved. This geometry is desirable for its relevance to experiment and also for comparison with theoretical results by other authors. In addition to cyclotron damping, Landau damping as well as electron–ion, electron–electron, and electron–neutral collisions are all included thus enabling the relative importance of these damping mechanisms to be evaluated. The dispersion relation that is obtained is used to explore the transition from Landau dominated damping to cyclotron dominated damping.

I. INTRODUCTION

The object of this paper is to investigate the damping of whistler waves (sometimes called helicon waves) in a homogeneous, magnetized, and bounded plasma. This is motivated by the use of radio frequency power in the production of dense plasmas for applications such as plasma processing. Particular attention is paid to examining the relative significance of various heating effects including collisional damping as well as the collisionless damping mechanisms such as Landau and cyclotron damping.

The effect of Landau damping on bounded whistler waves has been calculated previously using kinetic theory by Dolgopolov *et al.*,[1] and used to explain the strong damping they had observed in experiment.[2] Recently, Chen[3] used fluid theory with a kinetic correction to show that Landau damping could explain the high ionizing efficiency observed in experiments[4–6] and this result was invoked by Zhu and Boswell[7] to explain the selective excitation of the upper lasing level of Ar II. Because of the very low wave frequencies in these experiments, more than two orders of magnitude below the cyclotron frequency, cyclotron damping was quite legitimately ignored, although Landau and collisional damping were both included by Chen[8] and Shoji *et al.*[9]

Cyclotron damping of whistler waves is normally only considered when the wave frequency is close to the electron cyclotron frequency. At this frequency, the right-hand polarization of whistler waves makes for particularly efficient cyclotron damping.[10]

In this paper intermediate frequency whistler waves are modeled. Although the frequencies of these waves are well below the cyclotron frequency, the cyclotron resonance terms are retained in full since it will be shown that for high density plasmas, $\omega_p^2\omega/\Omega^3 \sim (c/v_T)^2$, the density dependent parallel wave number can be large enough to bring thermal electrons into cyclotron resonance.

For each of the collisionless damping mechanisms, the regions of velocity space, in which the electrons absorb the energy lost by the wave, can be calculated for the varying plasma parameters. Since these results are calculated for relatively low temperature plasmas they raise the possibility, when applied to partially ionized plasmas, of focusing energy on the most efficiently ionizing electrons for a cost effective radio frequency plasma source.

II. WAVE EQUATION

The spatial evolution of the electric and magnetic fields is given by Maxwell's equations

$$\nabla\times\mathbf{E}=-\frac{\partial\mathbf{B}}{\partial t}, \tag{1}$$

$$\nabla\times\mathbf{B}=\mu_0\mathbf{J}+\frac{1}{c^2}\frac{\partial\mathbf{E}}{\partial t}. \tag{2}$$

A. Cylindrical geometry

For a wave varying as $\exp(-i\omega t)$, the components of Eq. (1) in cylindrical geometry are

$$\frac{1}{r}\frac{\partial E_z}{\partial\phi}-\frac{\partial E_\phi}{\partial z}=i\omega B_r, \tag{3}$$

$$\frac{\partial E_r}{\partial z}-\frac{\partial E_z}{\partial r}=i\omega B_\phi, \tag{4}$$

$$\frac{1}{r}\frac{\partial}{\partial r}(rE_\phi)-\frac{1}{r}\frac{\partial E_r}{\partial\phi}=i\omega B_z, \tag{5}$$

while the components of Eq. (2) are

$$\frac{1}{r}\frac{\partial B_z}{\partial\phi}-\frac{\partial B_\phi}{\partial z}=\mu_0 J_r-\frac{i\omega}{c^2}E_r, \tag{6}$$

$$\frac{\partial B_r}{\partial z}-\frac{\partial B_z}{\partial r}=\mu_0 J_\phi-\frac{i\omega}{c^2}E_\phi, \tag{7}$$

Downloaded 08 Nov 2012 to 194.81.223.66. Redistribution subject to AIP license or copyright; see http://pop.aip.org/about/rights_and_permissions

$$\frac{1}{r}\frac{\partial}{\partial r}(rB_\phi)-\frac{1}{r}\frac{\partial B_r}{\partial \phi}=\mu_0 J_z-\frac{i\omega}{c^2}E_z. \tag{8}$$

B. Nonscalar conductivity

In the absence of collisions, the behavior of the velocity distribution of a particular plasma species is given by the Vlasov equation. For small amplitude waves this can be linearized about a Maxwellian equilibrium,

$$\frac{\partial f_1}{\partial t}+\mathbf{v}\cdot\frac{\partial f_1}{\partial x}+\frac{q}{m}\mathbf{v}\times\mathbf{B_0}\cdot\frac{\partial f_1}{\partial \mathbf{v}}=-\frac{q}{m}\mathbf{E}\cdot\frac{\partial f_0}{\partial \mathbf{v}}. \tag{9}$$

For high frequency waves we need only consider the response of the electron distribution to the electric field. Thermal effects parallel to the magnetic field (such as the Doppler shift) are retained in our calculation of the perturbed electron distribution function, while thermal effects perpendicular to the magnetic field (such as the finite Larmor radius) are neglected. Fourier transforming Eq. (9) in space and time, using cylindrical coordinates for velocity,

$$v_x=v_\perp\cos\theta,\quad v_y=v_\perp\sin\theta,$$

and writing f_1 as a Fourier series in θ, we obtain an infinite system of coupled equations for the Fourier components of the perturbed distribution. Ignoring finite Larmor radius effects decouples the equations and so only the three Fourier components which contribute to the electric currents need be considered:

$$i(\omega-\Omega-k_z v_z)f_{1-}=\frac{e\tilde{E}_- v_\perp}{m_e v_T^2}f_0, \tag{10}$$

$$i(\omega-k_z v_z)f_{1z}=\frac{2eE_z v_z}{m_e v_T^2}f_0, \tag{11}$$

$$i(\omega+\Omega-k_z v_z)f_{1+}=\frac{e\tilde{E}_+ v_\perp}{m_e v_T^2}f_0, \tag{12}$$

with

$$\tilde{E}_-=\frac{E_x-iE_y}{\sqrt{2}},\quad \tilde{E}_+=\frac{E_x+iE_y}{\sqrt{2}},$$

$$\Omega=\frac{eB_0}{m_e},\quad v_T^2=\frac{2k_BT}{m_e},$$

and

$$f_1(v_\perp,v_z,\theta)=f_{1z}(v_\perp,v_z)+\sqrt{2}f_{1-}(v_\perp,v_z)e^{i\theta}+\sqrt{2}f_{1+}(v_\perp,v_z)e^{-i\theta}.$$

The first velocity moment of the perturbed distribution multiplied by the charge of the species gives the perturbed electric current,

$$\tilde{J}_-=\frac{J_x-iJ_y}{\sqrt{2}}=-e2\pi\int_0^\infty dv_\perp\, v_\perp^2\int_{-\infty}^\infty dv_z\, f_{1-}=-i\frac{\epsilon_0\omega_p^2}{k_z v_T}Z\left(\frac{\omega-\Omega}{k_z v_T}\right)\tilde{E}_-, \tag{13}$$

$$J_z=-e2\pi\int_0^\infty dv_\perp\, v_\perp\int_{-\infty}^\infty dv_z\, v_z f_{1z}=-2i\epsilon_0\frac{\omega\omega_p^2}{k_z^2v_T^2}\left[1+\frac{\omega}{k_z v_T}Z\left(\frac{\omega}{k_z v_T}\right)\right]E_z, \tag{14}$$

$$\tilde{J}_+=\frac{J_x+iJ_y}{\sqrt{2}}=-e2\pi\int_0^\infty dv_\perp\, v_\perp^2\int_{-\infty}^\infty dv_z\, f_{1+}=-i\frac{\epsilon_0\omega_p^2}{k_z v_T}Z\left(\frac{\omega+\Omega}{k_z v_T}\right)\tilde{E}_+, \tag{15}$$

where

$$\omega_p^2=\frac{e^2n_e}{m_e\epsilon_0}.$$

Finally, noting that changing to cylindrical coordinates only modifies the phases of the right-hand and left-hand components of a vector,

$$J_-=\frac{J_r-iJ_\phi}{\sqrt{2}}=\tilde{J}_-e^{-i\phi},\quad E_-=\frac{E_r-iE_\phi}{\sqrt{2}}=\tilde{E}_-e^{-i\phi},$$
$$J_+=\frac{J_r+iJ_\phi}{\sqrt{2}}=\tilde{J}_+e^{i\phi},\quad E_+=\frac{E_r+iE_\phi}{\sqrt{2}}=\tilde{E}_+e^{i\phi}, \tag{16}$$

these currents can be combined with Maxwell's equations to give a set of linear equations for the components of the electromagnetic field.

The right-hand component is given by

$$G_-E_-=\partial_-(in_zE_z-cB_z), \tag{17}$$

where

$$G_-=1+\frac{\omega_p^2}{\omega k_z v_T}Z\left(\frac{\omega-\Omega}{k_z v_T}\right)-n_z^2$$

and

$$\partial_-=\frac{c}{\sqrt{2}\omega}\left(\frac{\partial}{\partial r}-\frac{i}{r}\frac{\partial}{\partial\phi}\right)=\frac{c}{\sqrt{2}\omega}\left(\frac{\partial}{\partial r}+\frac{m}{r}\right).$$

The left-hand component is given by

$$G_+E_+=\partial_+(in_zE_z+cB_z), \tag{18}$$

where

$$G_+=1+\frac{\omega_p^2}{\omega k_z v_T}Z\left(\frac{\omega+\Omega}{k_z v_T}\right)-n_z^2$$

and

Downloaded 08 Nov 2012 to 194.81.223.66. Redistribution subject to AIP license or copyright; see http://pop.aip.org/about/rights_and_permissions

$$\partial_+ = \frac{c}{\sqrt{2}\omega}\left(\frac{\partial}{\partial r}+\frac{i}{r}\frac{\partial}{\partial \phi}\right)=\frac{c}{\sqrt{2}\omega}\left(\frac{\partial}{\partial r}-\frac{m}{r}\right).$$

The parallel component is given by

$$G_z E_z=(1/r)[\partial_-(rcB_+)-\partial_+(rcB_-)], \tag{19}$$

where

$$G_z=1+2\frac{\omega_p^2}{k_z^2 v_T^2}\left[1+\frac{\omega}{k_z v_T}Z\left(\frac{\omega}{k_z v_T}\right)\right].$$

These equations are valid for any high frequency wave, but in this paper attention will be restricted to plasmas with $\omega_p \gg \Omega$ and waves with $\omega < \Omega$.

Completing the set of equations are those for the perturbed magnetic field,

$$G_- cB_- = \partial_-[in_z cB_z+(G_-+n_z^2)E_z], \tag{20}$$

$$G_+ cB_+ = \partial_+[in_z cB_z-(G_++n_z^2)E_z], \tag{21}$$

$$cB_z=(1/r)[\partial_+(rE_-)-\partial_-(rE_+)]. \tag{22}$$

Multiplying Eq. (22) by G_-G_+, eliminating G_-E_- [using Eq. (17)] and eliminating G_+E_+ [using Eq. (18)] gives an equation containing only E_z and B_z,

$$SL_m(cB_z)+G_+G_-cB_z-in_z DL_m(E_z)=0. \tag{23}$$

The differential operator L_m is

$$\begin{aligned} L_m(\psi) &= \frac{2}{r}\partial_-(r\partial_+\psi) \\ &= \frac{2}{r}\partial_+(r\partial_-\psi) \\ &= \frac{c^2}{\omega^2}\left(\frac{\partial^2\psi}{\partial r^2}+\frac{1}{r}\frac{\partial\psi}{\partial r}-\frac{m^2}{r^2}\psi\right), \end{aligned} \tag{24}$$

while S and D are

$$S=\frac{G_++G_-}{2}, \quad D=\frac{G_+-G_-}{2}.$$

Similarly, multiplying Eq. (19) by G_-G_+, eliminating G_-B_- [using Eq. (20)] and eliminating G_+B_+ [using Eq. (21)] gives another equation containing only E_z and B_z

$$in_z DL_m(cB_z)+Sn_z^2 L_m(E_z)+G_+G_-L_m(E_z)$$
$$+G_+G_zG_-E_z=0. \tag{25}$$

The eigenfunctions of the operator L_m are $J_m[\alpha(\omega r/c)]$ and $N_m[\alpha(\omega r/c)]$ with eigenvalue $-\alpha^2$. The requirement for finite fields at the origin excludes solutions based on the Neumann function.

The Hankel transforms of Eqs. (23) and (25) give Eq. (26)

$$\begin{pmatrix} S\alpha^2-G_+G_- & -in_z D\alpha^2 \\ in_z D\alpha^2 & (Sn_z^2+G_+G_-)\alpha^2-G_+G_zG_- \end{pmatrix}\begin{pmatrix} b \\ e \end{pmatrix} = \begin{pmatrix} 0 \\ 0 \end{pmatrix}, \tag{26}$$

where b and e are defined by

$$cB_z=bJ_m\left(\alpha\frac{\omega r}{c}\right), \quad E_z=eJ_m\left(\alpha\frac{\omega r}{c}\right).$$

The term $in_z D$ couples the rows of Eq. (26) and thus prevents pure TM (transverse magnetic) and TE (transverse electric) solutions from propagating along the cylinder. Setting $n_z=0$ does allow O-mode (TM) and X-mode (TE) solutions; however for a wave propagating along the cylinder n_z is clearly nonzero.

For solutions of this system of equations to exist the determinant must be zero. This condition gives a quadratic equation for the radial eigenvalue $-\alpha^2$.

$$\alpha^4(S+n_z^2)-\alpha^2[G_+G_-+S(G_z+n_z^2)]+G_+G_zG_-=0. \tag{27}$$

The existence of two roots is of course expected; perhaps less expected is the fact that both solutions are required if conducting wall boundary conditions are to be satisfied

$$cB_z=b_1J_m\left(\alpha_1\frac{\omega r}{c}\right)+b_2J_m\left(\alpha_2\frac{\omega r}{c}\right),$$

$$E_z=e_1J_m\left(\alpha_1\frac{\omega r}{c}\right)+e_2J_m\left(\alpha_2\frac{\omega r}{c}\right).$$

As a preliminary step note that the first row of Eq. (26) implies that

$$b_j=\frac{in_z D\alpha_j^2}{S\alpha_j^2-G_+G_-}e_j, \quad j=1,2. \tag{28}$$

Subtracting the product of G_+ with Eq. (17) from the product of G_- with Eq. (18) gives E_ϕ in terms of E_z and B_z,

$$G_+G_-iE_\phi = S\frac{c}{\omega}\left(\frac{\partial cB_z}{\partial r}-\frac{in_z m}{r}E_z\right)$$
$$-D\frac{c}{\omega}\left(in_z\frac{\partial E_z}{\partial r}-\frac{m}{r}cB_z\right). \tag{29}$$

At the conducting wall, both E_ϕ and E_z must be zero. This contrasts with the approach of Chen,[8] where, *a priori*, it is assumed that $E_z=0$ everywhere. Later in the same paper, a nonzero E_z is obtained from J_z in order to calculate Landau damping. Unfortunately, the E_z obtained by Chen does not vanish on the conducting wall. For the frequency regime in which we are interested, the nonexistence of any solution using only one root can be proven as follows.

If a solution consisting of a single α exists then, from the condition that $E_z=0$ at the wall, α must satisfy

$$J_m\left(\alpha\frac{\omega r_w}{c}\right)=0.$$

The condition that $E_\phi=0$ at the wall gives Eq. (30):

$$(Sb-Din_z e)\frac{\partial}{\partial r}J_m\left(\alpha\frac{\omega r}{c}\right)\Big|_{r=r_w}=0. \tag{30}$$

Downloaded 08 Nov 2012 to 194.81.223.66. Redistribution subject to AIP license or copyright; see http://pop.aip.org/about/rights_and_permissions

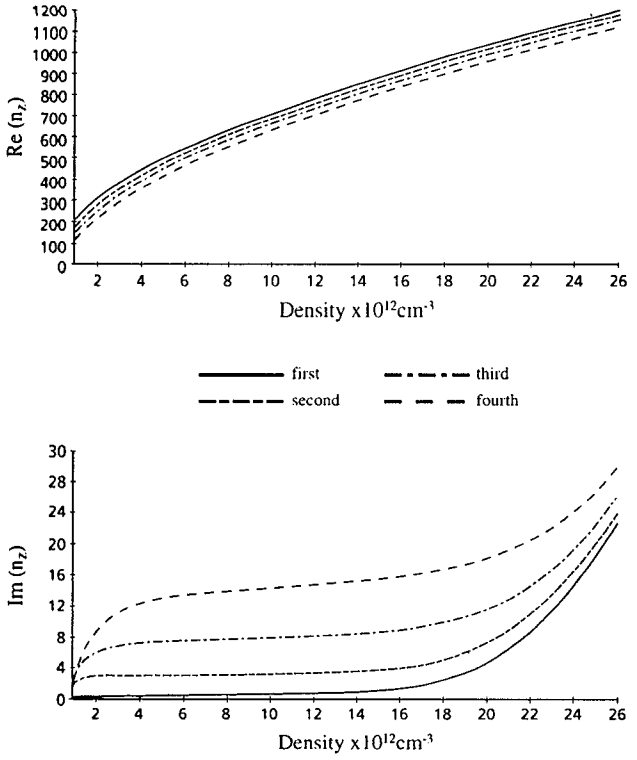

FIG. 1. Real and imaginary parts of n_z as functions of density for the first four radial modes corresponding to $m=1$. The plasma has a 10 cm radius, a temperature of 3 eV, and is in a magnetic field of 48.4 G. The wave frequency is 13.56 MHz ($\Omega/\omega=10$).

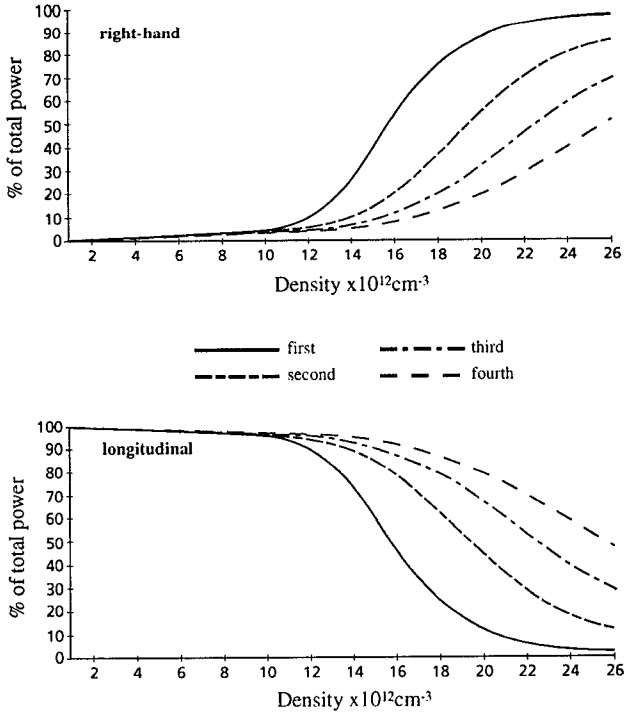

FIG. 2. Cyclotron and Landau damping as functions of density for the first four radial modes corresponding to $m=1$. The plasma has a 10 cm radius, a temperature of 3 eV, and is in a magnetic field of 48.4 G. The wave frequency is 13.56 MHz ($\Omega/\omega=10$).

Using Eq. (28) to eliminate e in Eq. (30) gives $b=0$ which from Eq. (28) implies $e=0$. Therefore no nonzero solution can be formed using only one root of Eq. (27).

The lack of single mode solutions to the conducting boundary problem is related to the lack of TE and TM modes in that it, also, is due to the term $n_z D$.

III. CONDUCTING WALL

Using both roots of Eq. (27) solutions to the conducting wall problem can be obtained for suitable values of G_+, G_z, and G_-.

Using Eq. (28) the magnetic field components b_1 and b_2 can be eliminated in favor of the electric field components e_1 and e_2. The boundary condition $E_z=0$ on the wall gives e_2 in terms of e_1. Applying the final condition $E_\phi=0$ on the wall gives the dispersion relation for the bounded wave

$$\alpha_1(G_+G_- - \alpha_2^2 S)J_m\left(\alpha_2\frac{\omega r_w}{c}\right)J'_m\left(\alpha_1\frac{\omega r_w}{c}\right)$$
$$-\alpha_2(G_+G_- - \alpha_1^2 S)J_m\left(\alpha_1\frac{\omega r_w}{c}\right)J'_m\left(\alpha_2\frac{\omega r_w}{c}\right)$$
$$=\frac{mc}{\omega r}(\alpha_2^2-\alpha_1^2)DJ_m\left(\alpha_2\frac{\omega r_w}{c}\right)J_m\left(\alpha_1\frac{\omega r_w}{c}\right). \quad (31)$$

Both Eq. (27), and Eq. (31) are transcendental in the parallel wave number k_z. ZERINT (a general, complex root, solver) is used to solve this system numerically for k_z.

It is found that for each m, a spectrum of k_z solutions exist, corresponding to different radial modes.

Whistler solutions are characterized by their polarization—predominantly right-handed (E_-)—and their direction of propagation—nearly parallel to the equilibrium magnetic field. These characteristics will be most easily found among solutions with E_- large and proportional to J_0. Using the Bessel function identities

$$\partial_+ J_m\left(\alpha\frac{\omega r}{c}\right)=-\frac{\alpha}{\sqrt{2}}J_{m+1}\left(\alpha\frac{\omega r}{c}\right), \quad (32)$$

$$\partial_- J_m\left(\alpha\frac{\omega r}{c}\right)=\frac{\alpha}{\sqrt{2}}J_{m-1}\left(\alpha\frac{\omega r}{c}\right), \quad (33)$$

it is clear that $m=1$ modes will have E_- proportional to J_0.

Setting $m=1$, the dependence of the first four radial modes on the plasma density can be calculated. The results for a 13.56 MHz wave propagating through a 3 eV plasma are plotted in Fig. 1. The equilibrium magnetic field used is 0.004 84 T to give a cyclotron frequency of 135.6 MHz (an order of magnitude larger than the wave frequency). For comparison: in their experiment Perry and Boswell[5] use the same wave frequency in a 0.005 T magnetic field.

The Landau damping rises rapidly at first, as the increasing n_z reduces the required velocity for particle resonance. At higher densities the increase in parallel conductivity is counterbalanced by the changing polarization of the electric field; the parallel component (E_z) decreases

Downloaded 08 Nov 2012 to 194.81.223.66. Redistribution subject to AIP license or copyright; see http://pop.aip.org/about/rights_and_permissions

and the right-hand component (E_-), increases. Finally as the density, and so n_z, continues to increase, cyclotron damping rises rapidly to become dominant. Continuing to raise the density increases the right-hand component of the electric field and reduces the required velocity for cyclotron resonance. Both effects lead to a further rise in cyclotron damping.

IV. POWER DISTRIBUTION BETWEEN RESONANCES

Since the applied frequency ω is real, the electromagnetic energy density T is independent of time

$$T=\tfrac{1}{2}(\epsilon_0\mathbf{E}^*\cdot\mathbf{E}+\mu_0\mathbf{H}^*\cdot\mathbf{H}), \tag{34}$$

and so employing Poynting's theorem:

$$\mathrm{Re}[\nabla\cdot(\mathbf{E}^*\times\mathbf{H})+\mathbf{E}^*\cdot\mathbf{J}]=0. \tag{35}$$

The electromagnetic power transferred from the wave to the plasma can now be calculated from the loss of Poynting flux, or the $\mathbf{E}^*\cdot\mathbf{J}$ gain of the plasma. Moreover, since the gain of the plasma separates naturally into Landau, cyclotron, and anomalous Doppler components, the relative importance of each effect can be calculated:

$$\begin{aligned}\mathrm{Re}(\mathbf{E}^*\cdot\mathbf{J})=&\mathrm{Im}\left[\frac{c\omega_p^2}{2v_T\omega n_z}Z\left(\frac{c(1-\Omega/\omega)}{v_T n_z}\right)\right]\epsilon_0|E_-|^2\\&+\mathrm{Im}\left\{\frac{2c^2\omega_p^2}{v_T^2\omega n_z^2}\left[1+\frac{c}{v_T n_z}Z\left(\frac{c}{v_T n_z}\right)\right]\right\}\epsilon_0|E_z|^2\\&+\mathrm{Im}\left[\frac{c\omega_p^2}{2v_T\omega n_z}Z\left(\frac{c(1+\Omega/\omega)}{v_T n_z}\right)\right]\epsilon_0|E_+|^2.\end{aligned} \tag{36}$$

The terms on the right-hand side of Eq. (36) give, respectively, the cyclotron damping, the Landau damping, and the anomalous Doppler damping.

These three damping effects occur at three distinct parallel velocities. Electrons traveling in the opposite direction to the wave at a velocity of $(\omega-\Omega)/k_z$ experience a frequency increased by the Doppler effect to the cyclotron frequency and cyclotron damp the right-hand polarization (E_-) which rotates in the same sense as the electrons. Electrons moving with the wave at the parallel phase velocity experience a constant field and Landau damp the parallel polarization (E_z). Finally, electrons moving faster than the phase velocity experience a wave with the opposite time dependence; the left-hand polarization (E_+) now rotating in the same sense as the electrons. Thus cyclotron resonance occurs for the left-hand polarization at a parallel velocity of $(\omega+\Omega)/k_z$ and is referred to as the anomalous Doppler resonance.

Using Eq. (36) the percentages of the total power lost from the wave that are due to cyclotron, Landau, and anomalous Doppler damping can be calculated. It is found that the power loss due to anomalous Doppler damping is negligible over the entire density range. This was to be expected since the electric field polarization became unsuitable for anomalous Doppler damping at a lower value of n_z than that required to provide a large enough Doppler shift to bring the left-hand polarized perturbation into resonance.

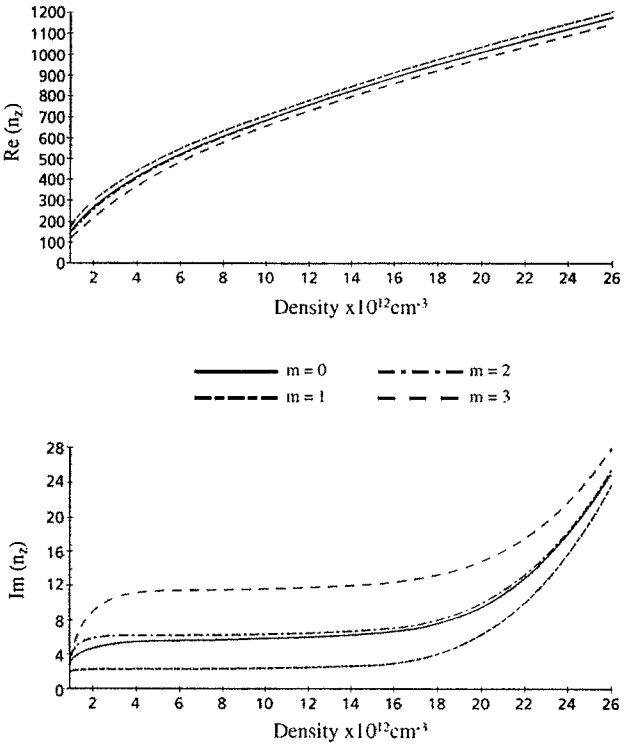

FIG. 3. Real and imaginary parts of n_z as functions of density for the lowest radial mode corresponding to $m=0\rightarrow3$. The plasma has a 5 cm radius, a temperature of 3 eV and is in a magnetic field of 48.4 G. The wave frequency is 13.56 MHz ($\Omega/\omega=10$).

A plot of the percentages of cyclotron and Landau damping for the same range of parameters as were used in Fig. 1 is given in Fig. 2, confirming the interpretation of Fig. 1 given above.

In Fig. 3 graphs are drawn for the first radial modes corresponding to $m=0\rightarrow3$. It can be seen from this figure that the $m=1$ solution which was chosen earlier has the lowest damping, particularly for densities around 1.6×10^{13} cm^{-3} and below, where we would expect damping to be dominated by Landau damping. As the density is increased to 2.5×10^{13} cm^{-3} and beyond, we would expect cyclotron damping to become dominant. In Fig. 3 we can see that the graphs of $\mathrm{Im}(n_z)$ obtained for a range of m values converge at these higher densities. Moving away from $m=1$, $m=0$ and $m=2$ have very similar behavior to each other showing heavier damping than the $m=1$ solution while the heaviest damping occurs in the $m=3$ case.

Figure 4 confirms that Landau damping is dominant in the density range (1.6×10^{13} cm^{-3} and below) which shows the strongest dependence of damping on m. The difference in damping experienced by the different m can be attributed primarily to differences in the amount of Landau damping.

From Eq. (36) Landau damping is proportional to $|E_z|^2$ while, for a whistler wave which is predominantly right-hand polarized, Eq. (19) implies that

Downloaded 08 Nov 2012 to 194.81.223.66. Redistribution subject to AIP license or copyright; see http://pop.aip.org/about/rights_and_permissions

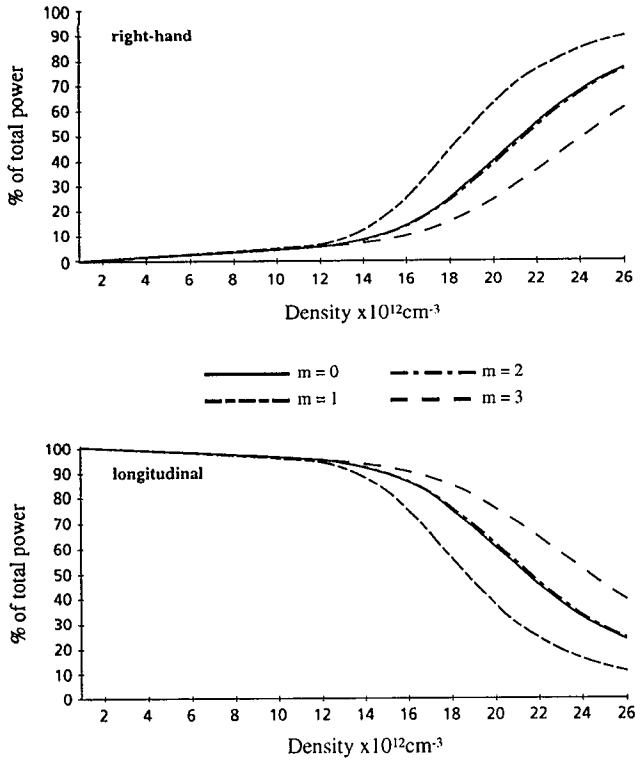

FIG. 4. Cyclotron and Landau damping as functions of density for the lowest radial mode corresponding to $m=0\rightarrow 3$. The plasma has a 5 cm radius, a temperature of 3 eV, and is in a magnetic field of 48.4 G. The wave frequency is 13.56 MHz ($\Omega/\omega=10$).

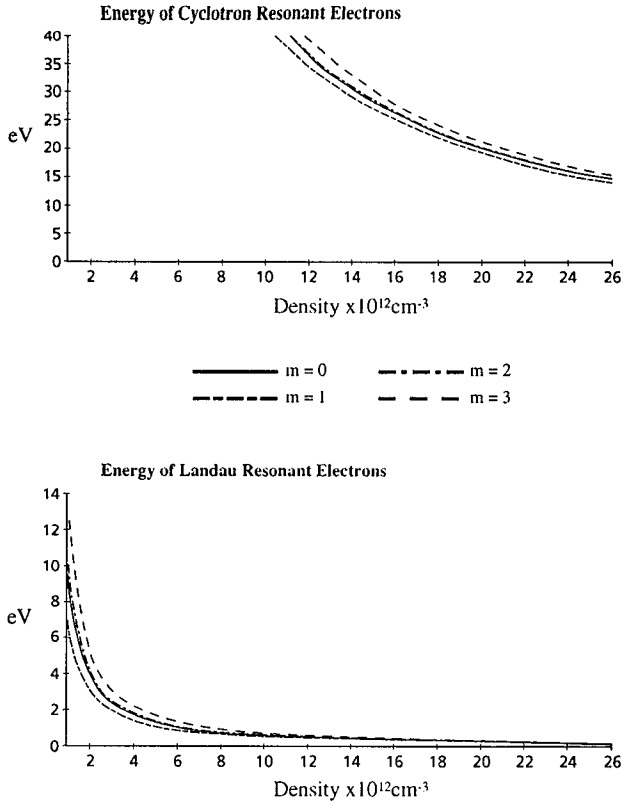

FIG. 5. Resonant parallel energies of the electrons performing cyclotron and Landau damping for $m=1\rightarrow 3$. The plasma has a 5 cm radius, a temperature of 3 eV, and is in a magnetic field of 48.4 G. The wave frequency is 13.56 MHz ($\Omega/\omega=10$).

$$E_z \approx \frac{-c}{G_z}\left(\frac{\partial}{\partial r}-\frac{m-1}{r}\right)B_- . \tag{37}$$

It is not surprising therefore that as we increase $|m-1|$ (Fig. 3) or the radial variation of the wave (Fig. 1), the strength of the Landau damping rises.

A. Damping region

The electrons responsible for Landau damping lie in a different region of velocity space from those responsible for cyclotron damping. When $\omega<\Omega$, the resonant parallel velocities are in opposite directions (parallel to the wave for Landau, antiparallel for cyclotron) and in the particular case $\omega=0.1\Omega$ the electron energies involved differ by nearly two orders of magnitude.

Identifying the region of velocity space in which power is being deposited is important because of the energy dependence of the efficiences of atomic processes such as excitation and ionization as well as the efficiencies of plasma processes such as current drive.

The parallel energies of the resonant electrons corresponding to Fig. 4 are plotted in Fig. 5. By comparing these graphs it can be seen that even when the cyclotron damping has become dominant the required resonant energy is still well above the thermal value.

Also of interest is the spatial location of the power deposition. To investigate this, the damping profiles for the $m=0\rightarrow 3$ are given in Figs. 6–9. The plasma density con-

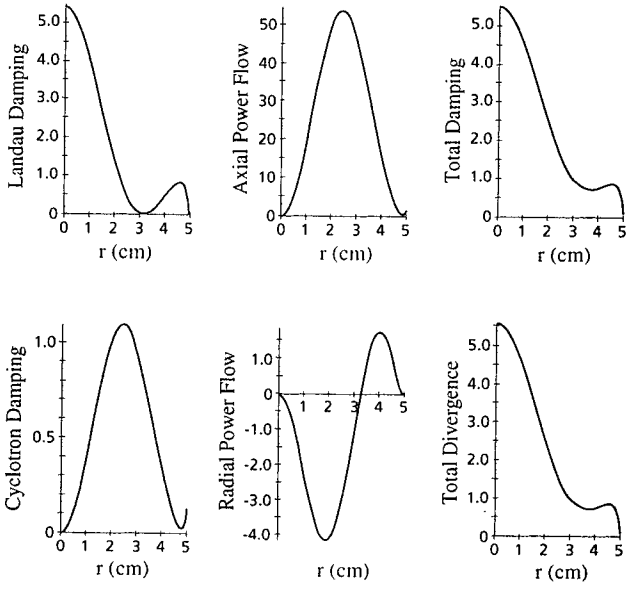

FIG. 6. Cyclotron and Landau damping profiles for the axially symmetric ($m=0$) mode. The plasma has a 5 cm radius, a density of 2×10^{13} cm^{-3}, a temperature of 3 eV, and is in a magnetic field of 48.4 G. The wave frequency is 13.56 MHz ($\Omega/\omega=10$).

Downloaded 08 Nov 2012 to 194.81.223.66. Redistribution subject to AIP license or copyright; see http://pop.aip.org/about/rights_and_permissions

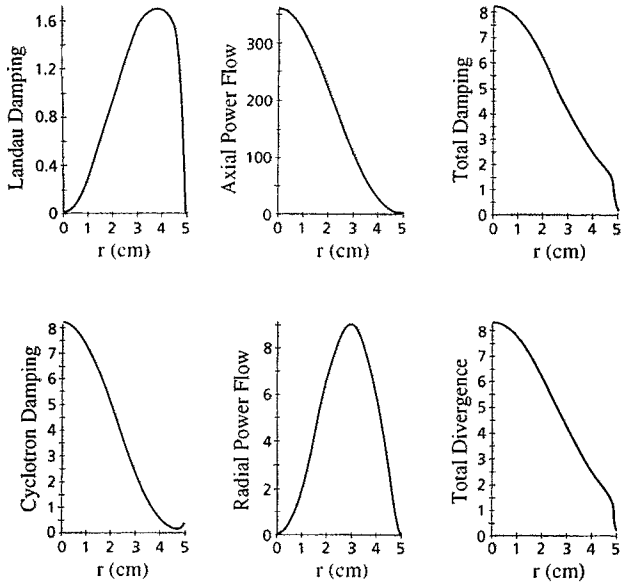

FIG. 7. Cyclotron and Landau damping profiles for the $m=1$ mode. The plasma has a 5 cm radius, a density of 2×10^{13} cm^{-3}, a temperature of 3 eV, and is in a magnetic field of 48.4 G. The wave frequency is 13.56 MHz ($\Omega/\omega=10$).

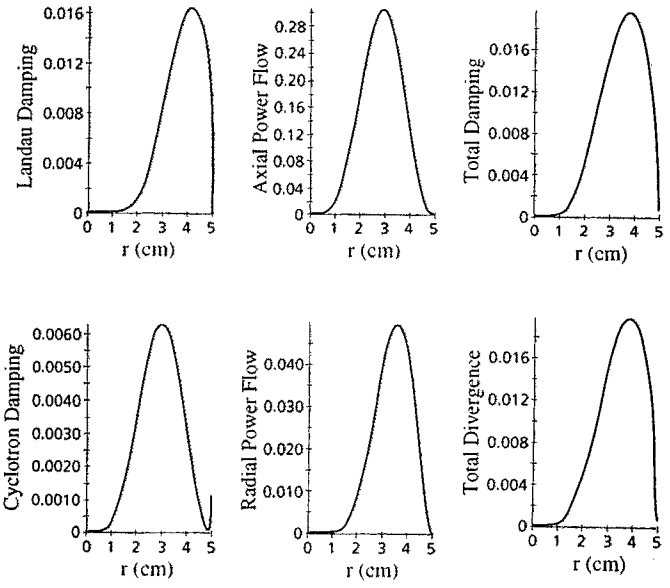

FIG. 9. Cyclotron and Landau damping profiles for the $m=3$ mode. The plasma has a 5 cm radius, a density of 2×10^{13} cm^{-3}, a temperature of 3 eV, and is in a magnetic field of 48.4 G. The wave frequency is 13.56 MHz ($\Omega/\omega=10$).

sidered is 2×10^{13} cm^{-3}, with the rest of the parameters taken from Fig. 3. It should be noted that the power fluxes in Figs. 6–9 are not normalized!

In Fig. 6 the Landau damping accounts for 61.3% of the total damping and is peaked on the axis, while the cyclotron damping (38.7%) is strongest at a radius of 2.4 cm. This is as expected for the $m=0$ case as E_z behaves as J_0 and E_- behaves as J_1.

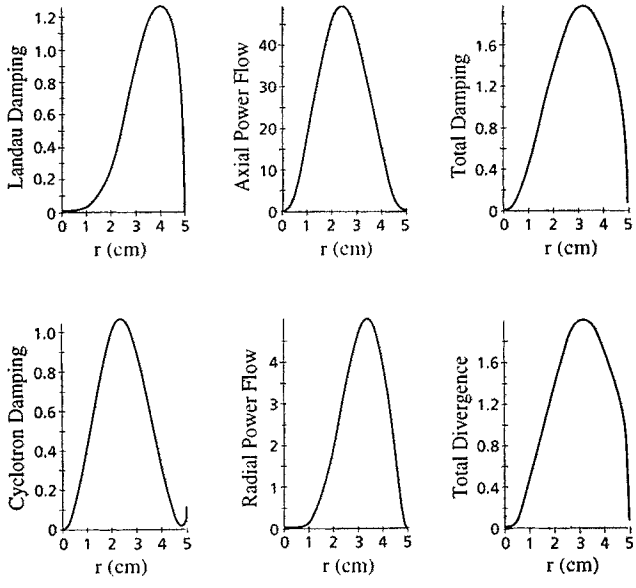

FIG. 8. Cyclotron and Landau damping profiles for the $m=2$ mode. The plasma has a 5 cm radius, a density of 2×10^{13} cm^{-3}, a temperature of 3 eV, and is in a magnetic field of 48.4 G. The wave frequency is 13.56 MHz ($\Omega/\omega=10$).

The roles of Landau and cyclotron damping are interchanged in the $m=1$ (Fig. 7) case with the cyclotron damping peaked on axis and accounting for 62.5% of the total damping while the Landau damping (37.5%) is strongest at a radius of 3 cm. This interchange of profiles is expected since E_- now behaves as J_0 while E_z behaves as J_1.

Finally profiles for $m=2$ are given in Fig. 8. It will be remembered from Fig. 3 that this case produces an almost identical value of n_z to that obtained in the $m=0$ case. It will also be remembered from Fig. 4 that the fractions of Landau damping (62%) and cyclotron damping (38%) were almost identical to those obtained for $m=0$. Despite these similarities, the damping profiles are very different. The maximum damping for $m=0$ occurs on the axis where $m=2$ has no electric field and so no damping.

B. Radial power flow

It might have been expected that, in a cylindrically bounded plasma, the perturbing fields would form standing waves in the radial direction with no net radial power flow; just as they do in the absence of dissipation. To understand why the radial power flows in Figs. 6–9 are nonzero we must consider the damping profiles in these figures. From Eq. (36) the cyclotron damping is proportional to $|E_-|^2$ and so the cyclotron damping profile varies as $|J_{m-1}|^2$; since the whistler wave is right-hand polarized, the transverse electric field is dominated by $|E_-|$ (except at the boundary where E_+ and E_- are equal) giving an axial power flow with almost identical profile. Landau damping is proportional to $|E_z|^2$ and so has a different profile ($|J_m|^2$). This difference in profiles implies the existence of a nonzero radial component of the power flow.

Downloaded 08 Nov 2012 to 194.81.223.66. Redistribution subject to AIP license or copyright; see http://pop.aip.org/about/rights_and_permissions

As an example, consider the case $m=0$; where strong Landau damping occurs on the axis, implying a significant net inflow of power to this region. Since there is no axial power flow in this region, the influx of power must be from the radial direction. This interpretation is confirmed by the plot of radial power flow.

As a further check, the divergence of both power flows are summed and plotted and compared with a plot of the sum of cyclotron and Landau damping. As expected from Eq. (36), these plots match.

V. DIELECTRIC WALL

When the plasma is bounded by a nonconducting wall, obtaining the boundary conditions from the continuity of the tangential electric field requires the calculation of the electric field in the dielectric.

For a dielectric constant ϵ,

$$S=G_{-,d}=G_{+,d}=\epsilon-n_z^2, \tag{38}$$

$$D=0, \quad G_{z,d}=\epsilon. \tag{39}$$

Substituting these values in Eq. (27) gives

$$\alpha^2=\epsilon-n_z^2.$$

For the plasma parameters considered in this paper $n_z^2 \gg \epsilon$ for glass or vacuum, and so

$$\alpha \approx i n_z.$$

The electric and magnetic fields in the dielectric therefore behave as modified Bessel functions, reflecting the fact that the wave is evanescent in these materials.

A. Thick dielectric wall

For a thick dielectric wall, defined by $|k_z(r_{w2}-r_{w1})| \gg 1$ only modified Bessel functions of the second kind (K_m) need be considered. Modified Bessel functions of the first kind (I_m) are excluded by the requirement that **E** and **B** tend to zero as r tends to infinity.

At the plasma edge, the tangential components of **E** and **B** are continuous. The continuity of E_z at the dielectric wall (at radius r_{w1}) implies

$$e_1 J_m\left(\alpha_1 \frac{\omega r_{w1}}{c}\right)+e_2 J_m\left(\alpha_2 \frac{\omega r_{w1}}{c}\right)=e_3 K_m(k_z r_{w1}) \tag{40}$$

and the continuity of B_z implies

$$b_1 J_m\left(\alpha_1 \frac{\omega r_{w1}}{c}\right)+b_2 J_m\left(\alpha_2 \frac{\omega r_{w1}}{c}\right)=b_3 K_m(k_z r_{w1}). \tag{41}$$

These equations, when combined with Eq. (28), specify the fields in the dielectric in terms of the field components in the plasma, e_1 and e_2. The continuity of E_ϕ

$$\frac{b_1}{\alpha_1} J'_m\left(\alpha_1 \frac{\omega r_{w1}}{c}\right)+\frac{b_2}{\alpha_2} J'_m\left(\alpha_2 \frac{\omega r_{w1}}{c}\right)-\frac{im}{k_z r_{w1}} \times\left[\left(\frac{G_z}{\alpha_1^2}-1\right) e_1 J_m\left(\alpha_1 \frac{\omega r_{w1}}{c}\right)+\left(\frac{G_z}{\alpha_2^2}-1\right) e_2 J_m\left(\alpha_2 \frac{\omega r_{w1}}{c}\right)\right] =\frac{ime_3}{k_z r_{w1}} K_m(k_z r_{w1})-\frac{b_3}{n_z} K'_m(k_z r_{w1}) \tag{42}$$

and of B_ϕ

$$iG_z\left[\frac{e_1}{\alpha_1} J'_m\left(\alpha_1 \frac{\omega r_{w1}}{c}\right)+\frac{e_2}{\alpha_2} J'_m\left(\alpha_2 \frac{\omega r_{w1}}{c}\right)\right] -\frac{mcn_z}{\omega r_{w1}}\left[\frac{b_1}{\alpha_1^2} J_m\left(\alpha_1 \frac{\omega r_{w1}}{c}\right)+\frac{b_2}{\alpha_2^2} J_m\left(\alpha_2 \frac{\omega r_{w1}}{c}\right)\right] =\frac{m}{k_z r_{w1}} b_3 K_m(k_z r_{w1}), \tag{43}$$

when combined with Eq. (28) gives two equations in two unknowns e_1 and e_2. This system of equations is solved numerically using ZERINT.

B. Dielectric layer between plasma and conducting wall

Introduction of a conducting wall some distance from the plasma edge requires the inclusion of I_m in the solutions for the perturbed fields, giving two more degrees of freedom.

In Eqs. (40) and (42) $e_3 K_m(k_z r_{w1})$ is replaced by $e_3 K_m(k_z r_{w1})+e_4 I_m(k_z r_{w1})$, while the requirement that E_z disappears on a conducting wall at radius r_{w2} implies

$$e_4=-\frac{K_m(k_z r_{w2})}{I_m(k_z r_{w2})} e_3. \tag{44}$$

In Eqs. (41) and (43) $b_3 K_m(k_z r_{w1})$ is replaced by $b_3 K_m(k_z r_{w1})+b_4 I_m(k_z r_{w1})$ and in Eq. (42) $b_3 K'_m(k_z r_{w1})$ is replaced by $b_3 K'_m(k_z r_{w1})+b_4 I'_m(k_z r_{w1})$, while the requirement that E_ϕ disappears on a conducting wall implies

$$b_4=-\frac{K'_m(k_z r_{w2})}{I'_m(k_z r_{w2})} b_3. \tag{45}$$

As the thickness of the dielectric layer is increased, the solution will return to the thick dielectric wall form. In Fig. 10 the dependence of n_z on the thickness of the dielectric layer is shown for whistler waves with $m=0 \rightarrow 3$ in a moderate density (10^{12} cm^{-3}) plasma.

Although a conducting wall within a couple of centimeters of the plasma has a significant effect on n_z, this effect disappears rapidly as the wall is moved further from the plasma. In Fig. 10 n_z, typically, reaches its asymptotic value at a wall radius of 8 cm or less.

Since whistler waves in higher density plasmas have larger values of n_z, their electric fields decay more rapidly in the dielectric. It is therefore expected that the effect of a conducting wall at a fixed distance from the plasma will become insignificant as the plasma density is increased. In order to verify this, the refractive index n_z is plotted against density in Fig. 11 for four different conducting wall positions, ranging from 1 mm from the plasma edge to 3 cm from the edge. As the density increases, the four graphs

Downloaded 08 Nov 2012 to 194.81.223.66. Redistribution subject to AIP license or copyright; see http://pop.aip.org/about/rights_and_permissions

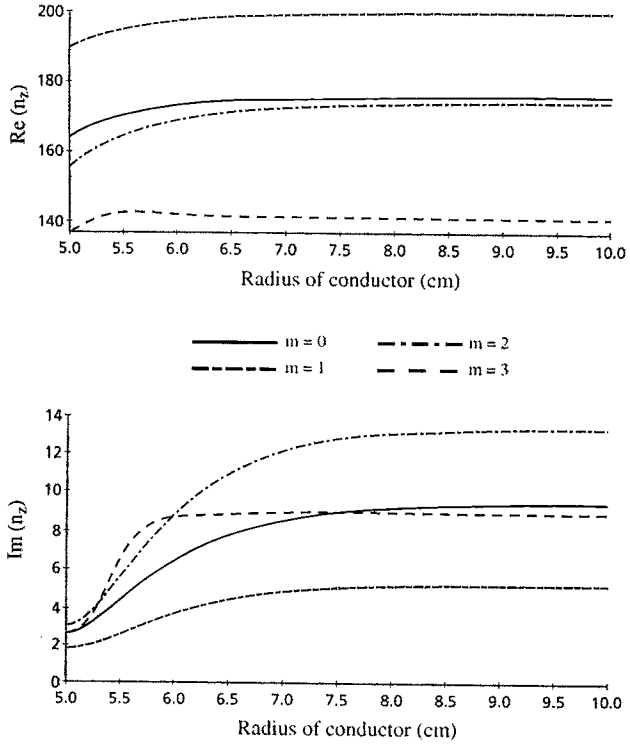

FIG. 10. Real and imaginary parts of n_z for $m=0\rightarrow 3$ as a function of the position of the conducting wall. The plasma has a 5 cm radius, a temperature of 3 eV, a density of 10^{12} cm^{-3}, and is in a magnetic field of 48.4 G. The wave frequency is 13.56 MHz ($\Omega/\omega=10$).

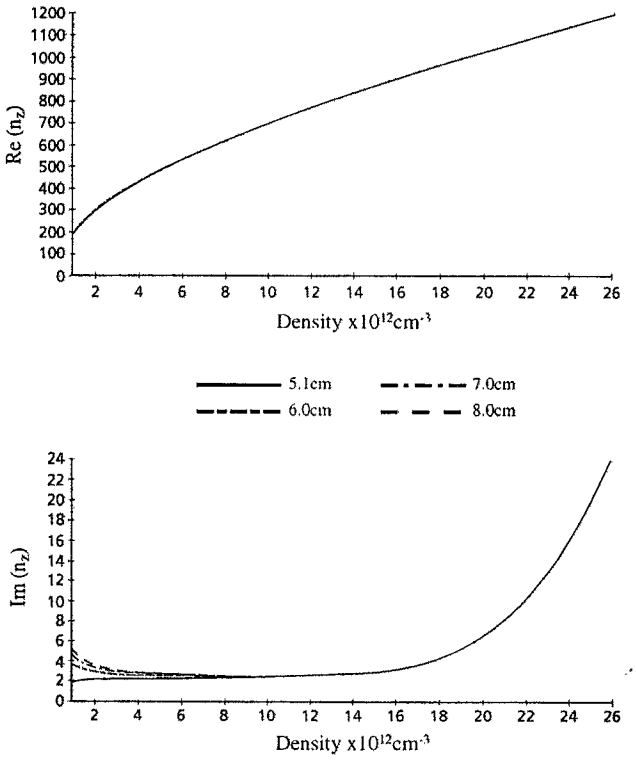

FIG. 11. Real and imaginary parts of n_z as functions of density for four different positions of the conducting wall. The plasma has a 5 cm radius, a temperature of 3 eV, and is in a magnetic field of 48.4 G. The wave frequency is 13.56 MHz ($\Omega/\omega=10$).

coalesce, showing that even 1 mm from the plasma edge the conducting wall ceases to perturb the wave.

VI. COLLISIONS

The effect of collisions on the perturbed velocity distribution is modeled using the BGK (Bhatnagar, Gross, and Krook, Ref. 11) collision term:

$$\left(\frac{Df_e}{Dt}\right)_c=\nu_{ee}(F_e-f_e)+\nu_{ei}(\bar{F}_e-f_e).$$

This describes the relaxation of the electron distribution function to thermal equilibrium with itself F_e at a rate given by the electron–electron collision frequency (ν_{ee}) and to thermal equilibrium with the ions $\bar{F}_e$ at a rate given by the electron–ion collision frequency (ν_{ei}).

The collision frequencies used in this theory are average values, i.e., calculated for particles moving at thermal velocities. The velocity dependence of collision frequencies is ignored.

Here $\bar{F}_e$ is chosen so that electron–ion collisions conserve charge, while F_e is chosen so that electron–electron collisions conserve charge (qn), momentum ($mn\mathbf{u}$), and energy (T),

$$\bar{F}_e=\left(1+\frac{n_1}{n_0}\right)f_0, \tag{46}$$

$$F_e=\left[1+\frac{n_1}{n_0}+2\,\frac{\mathbf{u}\cdot\mathbf{v}}{v_T^2}+\frac{T_1}{T_0}\left(\frac{v^2}{v_T^2}-\frac{3}{2}\right)\right]f_0. \tag{47}$$

Equating the linearized Vlasov operator to the linearized BGK collision operator gives

$$\frac{\partial f_1}{\partial t}+\mathbf{v}\cdot\frac{\partial f_1}{\partial \mathbf{x}}-\frac{e}{m_e}\mathbf{v}\times\mathbf{B}_0\cdot\frac{\partial f_1}{\partial \mathbf{v}}$$
$$=-\frac{e}{m_e}\mathbf{E}\cdot\frac{\partial f_0}{\partial \mathbf{v}}+\nu_{ee}(F_e-f_0-f_1)+\nu_{ei}(\bar{F}_e-f_0-f_1). \tag{48}$$

Fourier transforming Eq. (48) in space and time, using cylindrical coordinates for velocity, and ignoring finite Larmor radius effects, the three Fourier components which contribute to the electric currents are

$$i(\tilde{\omega}-\Omega-k_z v_z)f_{1-}=-\left(\nu_{ee}u_--\frac{eE_-}{m_e}\right)\frac{v_\perp}{v_T^2}f_0, \tag{49}$$

$$i(\tilde{\omega}-k_z v_z)f_{1z}=-\left\{2\left(\nu_{ee}u_z-\frac{eE_z}{m_e}\right)\frac{v_\perp}{v_T^2}+\nu_{ee}\right.$$
$$\left.\times\left[\frac{n_1}{n_0}+\frac{T_1}{T_0}\left(\frac{v^2}{v_T^2}-\frac{3}{2}\right)\right]+\nu_{ei}\frac{n_1}{n_0}\right\}f_0, \tag{50}$$

$$i(\tilde{\omega}+\Omega-k_z v_z)f_{1+}=-\left(\nu_{ee}u_+-\frac{eE_+}{m_e}\right)\frac{v_\perp}{v_T^2}f_0, \tag{51}$$

$$\tilde{\omega}=\omega+i(\nu_{ei}+\nu_{ee}).$$

Downloaded 08 Nov 2012 to 194.81.223.66. Redistribution subject to AIP license or copyright; see http://pop.aip.org/about/rights_and_permissions

Note that since the right- and left-hand components are unaffected by density or energy conservation and do not themselves contribute to the density or energy perturbations, only their first velocity moments need be calculated. Solving the resultant linear equations for u_- and u_+ and multiplying by the charge gives the perturbed current components

$$J_- = -i \frac{\epsilon_0 \omega_p^2 Z[(\tilde{\omega}-\Omega)/k_z v_T]}{k_z v_T + i\nu_{ee} Z[(\tilde{\omega}-\Omega)/k_z v_T]} E_- \tag{52}$$

and

$$J_+ = -i \frac{\epsilon_0 \omega_p^2 Z[(\tilde{\omega}+\Omega)/k_z v_T]}{k_z v_T + i\nu_{ee} Z[(\tilde{\omega}+\Omega)/k_z v_T]} E_+ . \tag{53}$$

However f_{1z} is affected by, and determines the perturbed density and energy as well as the parallel component of velocity

$$\frac{n_1}{n_0} = \frac{1}{n_0} \int f_{1z}\, d^3v, \tag{54}$$

$$\frac{u_z}{v_T} = \frac{1}{n_0 v_T} \int v_z f_{1z}\, d^3v, \tag{55}$$

$$\frac{3}{2}\left(\frac{T_1}{T_0} + \frac{n_1}{n_0}\right) = \frac{1}{n_0 v_T^2} \int v^2 f_{1z}\, d^3v. \tag{56}$$

On performing the velocity integrals, Eqs. (54) to (56) give three linear equations in three unknowns.

$$\mathbf{A} \cdot \mathbf{x} = \mathbf{y}, \tag{57}$$

where

$$\mathbf{A} = \begin{pmatrix} 1 + i\frac{\nu_{ee}+\nu_{ei}}{k_z v_T} Z & -i\frac{\nu_{ee}}{k_z v_T} Z' & i\frac{\nu_{ee}}{4k_z v_T} Z'' \\ -i\frac{\nu_{ee}+\nu_{ei}}{2k_z v_T} Z' & 1 - i\frac{\nu_{ee}\tilde{\omega}}{k_z^2 v_T^2} Z' & i\frac{\nu_{ee}\tilde{\omega}}{4k_z^2 v_T^2} Z'' \\ i\frac{\nu_{ee}+\nu_{ei}}{6k_z v_T} Z'' & i\frac{\nu_{ee}\tilde{\omega}}{3k_z^2 v_T^2} Z'' & 1 + i\frac{\nu_{ee}}{k_z v_T}\left(Z + \frac{Z''}{3} + \frac{Z^{IV}}{24}\right) \end{pmatrix}$$

and

$$\mathbf{x} = \begin{pmatrix} \frac{n_1}{n_0} \\ \frac{u_z}{v_T} \\ \frac{T_1}{T_0} \end{pmatrix}, \quad \mathbf{y} = -i\frac{eE_z}{m k_z v_T^2} \begin{pmatrix} Z' \\ \frac{\tilde{\omega}}{k_z v_T} Z' \\ -\frac{\tilde{\omega}}{3k_z v_T} Z'' \end{pmatrix}.$$

The current parallel to the equilibrium magnetic field can now be calculated by inverting Eq. (57)

$$J_z = q n_0 v_T \frac{u_z}{v_T}.$$

The modified currents give rise to modified G_-, G_z, and G_+:

$$G_- = 1 + \frac{\omega_p^2 Z[(\tilde{\omega}-\Omega)/k_z v_T]}{\omega\{k_z v_T + i\nu_{ee} Z[(\tilde{\omega}-\Omega)/k_z v_T]\}} - n_z^2, \tag{58}$$

$$G_+ = 1 + \frac{\omega_p^2 Z[(\tilde{\omega}+\Omega)/k_z v_T]}{\omega\{k_z v_T + i\nu_{ee} Z[(\tilde{\omega}+\Omega)/k_z v_T]\}} - n_z^2, \tag{59}$$

$$G_z = 1 - \frac{\omega_p^2}{\omega k_z v_T}\left[\left(M_{21} + \frac{\tilde{\omega}}{k_z v_T} M_{22}\right) Z' - \frac{\tilde{\omega}}{3k_z v_T} Z'' M_{23}\right], \tag{60}$$

where the matrix $\mathbf{M}$ is the inverse of $\mathbf{A}$.

The analysis from Eq. (23) onwards is still valid with the new form of G with the exception of Eq. (36) where now Eqs. (52) and (53) must be used in Eq. (35), and the power dissipation resolved only into longitudinal, left- and right-handed rather than Landau, anomalous Doppler, and cyclotron.

In Fig. 12 the net effect of collisions is to increase the total damping. It can also be seen that the collisional damping tends to smooth the variation of damping with density, blurring the transition from Landau to cyclotron damping.

The shape of the collisionless result is dictated by the velocity space resonance conditions. As n_z increases, a rapid rise in Landau damping is followed by a period of almost constant damping until n_z reaches the threshold for cyclotron damping, whereupon a second rapid rise in damping occurs.

Since collisional damping does not rely on velocity space resonances, it can give rise to significant power absorption of the right-hand polarization at densities well below those required for the Doppler shifted cyclotron damping. This can be seen in Fig. 13, where at low density around 10% of the power dissipated is lost collisionally.

The collisional element of the damping rises steadily as the collision frequency, itself an almost linear function of density, with no resonance behavior. At the same time, by scattering electrons out of resonance with the wave, collisions reduce the strength of Landau and cyclotron damp-

Downloaded 08 Nov 2012 to 194.81.223.66. Redistribution subject to AIP license or copyright; see http://pop.aip.org/about/rights_and_permissions

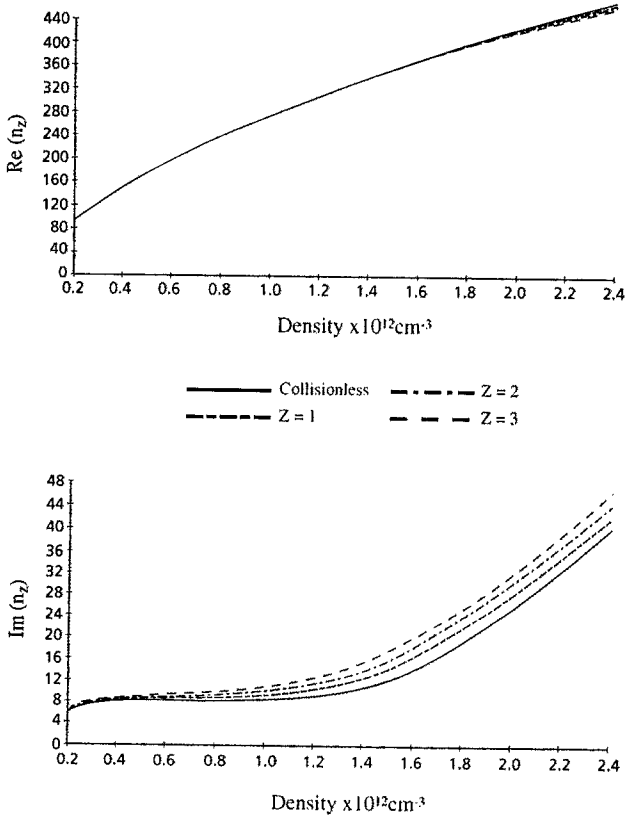

FIG. 12. Real and imaginary parts of n_z as functions of density for three values of the ion charge; the collisionless values (solid line) are included for comparison. The plasma has a 5 cm radius, a temperature of 9 eV, and is in a magnetic field of 29 G. The wave frequency is 13.56 MHz ($\Omega/\omega=6$).

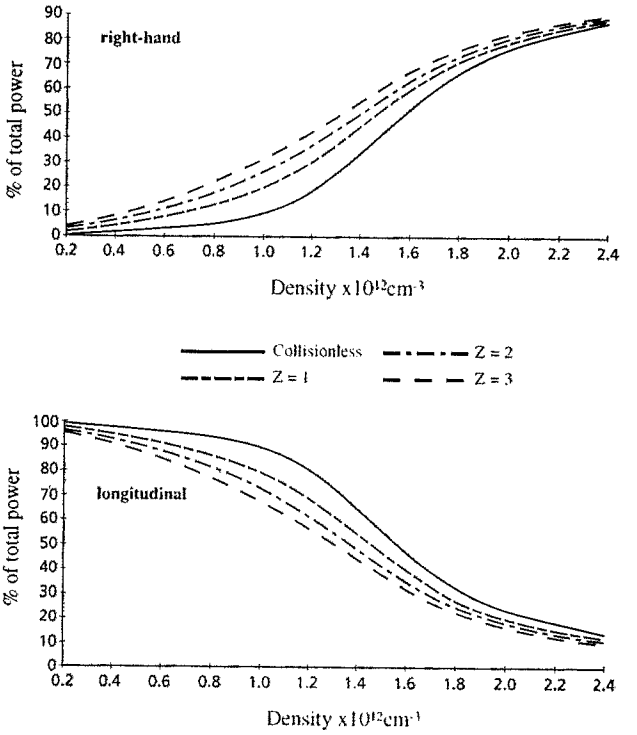

FIG. 13. Right-handed and longitudinal components of the damping for three values of the ion charge; the collisionless values (solid line) are included for comparison. The plasma has a 5 cm radius, a temperature of 9 eV, and is in a magnetic field of 29 G. The wave frequency is 13.56 MHz ($\Omega/\omega=6$).

ing. This is consistent with the collisional flattening in Fig. 13 of the graphs of both the right-hand and longitudinal components of the power loss.

A. Neutrals

Both electron–neutral and electron–ion collisions involve scattering of electrons by slow moving massive particles. Exploiting this similarity, an estimate of the effect of electron–neutral collisions can be made.

The cross section for momentum transfer collisions between electrons and neutrals is dependent on the neutral species and the electron temperature. For 9 eV electrons colliding with argon neutrals, the cross section is 1.8×10^{-15} cm^2.[12] Multiplying the cross section by the density of neutrals and the thermal velocity of the electrons gives the electron–neutral collision frequency. Comparing the electron-neutral collision frequency with the electron-ion collision frequency gives the ratio

$$\frac{\nu_{en}}{\nu_{ei}}\approx 0.1\,\frac{n_n}{n_e Z}, \tag{61}$$

where Z is the ion charge, and n_n and n_e are the neutral and electron densities, respectively.

From Eq. (61) it can be seen that, at low temperature, collisions with neutral particles can be ignored unless the neutral density is higher than the electron density.

When electron–neutral collisions are significant, they can be incorporated in the BGK collision model as an addition to the electron–ion collision term. Such an addition corresponds to replacing the ion charge Z (cf. Figs. 12 and 13) with an effective charge Z_{eff},

$$Z_{\text{eff}}=Z+0.1\,\frac{n_n}{n_e}. \tag{62}$$

If, for example, in Figs. 12 and 13 the ion charge was one and the neutral density was ten times the electron density, then the curves labeled $Z=2$ would be the appropriate ones to consult.

Both ions and neutrals are modeled as having the same temperature as the electrons. This approximation does not affect the collision frequencies or scattering, and is necessary for energy balance in the equilibrium.

Calculating the effects on wave propagation of ionization of neutrals and further ionization of ions would require a far more sophisticated collision operator.

VII. LENGTH SCALES

The results given in this report were obtained for 13.56-MHz waves. Therefore, the corresponding damping length is approximately

Downloaded 08 Nov 2012 to 194.81.223.66. Redistribution subject to AIP license or copyright; see http://pop.aip.org/about/rights_and_permissions

$$L=\frac{352}{\mathrm{Im}(n_z)}\ \mathrm{cm}. \tag{63}$$

When the real part of n_z is much greater than the imaginary part, it also makes sense to calculate the wavelength

$$\lambda=\frac{2211}{\mathrm{Re}(n_z)}\ \mathrm{cm}. \tag{64}$$

If we apply Eqs. (63) and (64) to the results given in Fig. 12 we find that when the density reaches 2.4×10^{12} cm^{-3} the axial wavelength of the collisionless solution is 4.6 cm and the damping length is 8.7 cm.

VIII. CONCLUSIONS

Whistler waves, even when the wave frequency is well below the cyclotron frequency, can still undergo strong cyclotron damping due to Doppler effects when the density exceeds a critical value. Because of the electric field polarization, this is the only collisionless damping mechanism available to a whistler wave propagating parallel to the magnetic field. However, for waves propagating in a bounded plasma, Landau damping is possible and does not require such a large n_z. Even so, when a large n_z is available, the cyclotron resonance can still be the dominant damping mechanism.

Both of these collisionless mechanisms concentrate the power damped from the wave on to electrons with particular parallel velocities; ω/k_z in the case of Landau damping and $(\omega-\Omega)/k_z$ in the case of cyclotron damping. By focusing power on electrons with particular energies, non-equilibrium effects such as anomalously high ionization efficiencies[4] and superthermal tails in the electron distribution,[13] have been found experimentally. Although these experiments invoked Landau damping, cyclotron damping should produce similar effects, either for higher frequencies, sufficiently dense plasmas or lower magnetic fields.

The large values of n_z obtained for whistler waves in dense plasmas not only facilitates cyclotron damping but also reduces the effects of external conducting surfaces by increasing the evanescence of the wave outside the plasma.

For low temperature plasmas, collisions are an important source of wave damping. Collisions become the dominant damping mechanism in two distinct regimes. First, when there is no competition from other damping mechanisms; this occurs when n_z is too small for cyclotron or Landau damping. Second, when the collision frequency exceeds the cyclotron frequency; this not only causes large collisional damping, but also reduces the collisionless damping by scattering particles out of resonance before they can be accelerated by the wave.

Between the two collision dominated regimes there is still a window for Doppler shifted cyclotron damping even in low temperature plasmas.

For $\omega\ll\Omega$, whistler waves become strongly cyclotron damped as the density approaches $\omega_p^2\omega/\Omega^3\sim(c/v_T)^2$.

ACKNOWLEDGMENTS

We would like to thank A. C. Riviere for his interest and encouragement, and T. J. Martin for providing the complex root finding code ZERINT that was used in this research.

This research was supported by the U.K. Department of Trade and Industry and Euratom and by AEA Technology's internally funded research program.

[1] V. V. Dolgopolov, A. I. Ermakov, N. I. Nazarov, K. N. Stepanov, and V. T. Tolok, Nucl. Fusion **3**, 251 (1963).
[2] N. I. Nazarov, A. I. Ermakov, V. V. Dolgopolov, K. N. Stepanov, and V. T. Tolok, Nucl. Fusion **3**, 255 (1963).
[3] F. F. Chen, in *Proceedings of the 1987 International Conference on Plasma Physics, Kiev* (World Scientific, Singapore, 1987), Vol. 2, p. 1378.
[4] R. W. Boswell, Plasma Phys. Controlled Fusion **26**, 1147 (1984).
[5] A. J. Perry and R. W. Boswell, Appl. Phys. Lett. **55**, 148 (1989).
[6] A. Komori, T. Shoji, K. Miyamoto, J. Kawai, and Y. Kawai, Phys. Fluids B **3**, 893 (1991).
[7] P. Zhu and R. W. Boswell, J. Appl. Phys. **68**, 1981 (1990).
[8] F. F. Chen, Plasma Phys. Controlled Fusion **33**, 339 (1991).
[9] T. Shoji, Y. Sakawa, S. Nakazawa, K. Kadota, and T. Sato, Plasma Sources Sci. Technol. **2**, 5 (1993).
[10] J. E. Stevens, J. L. Cecchi, Y. C. Huang, and R. L. Jarecki, Jr, J. Vac. Sci. Technol. A **9**, 696 (1991).
[11] P. L. Bhatnagar, E. P. Gross, and M. Krook, Phys. Rev. **94**, 511 (1954).
[12] A. Von Engel, *Ionized Gases*, 2nd ed. (Clarendon, Oxford, 1965), p. 33.
[13] P. Zhu and R. W. Boswell, Phys. Fluids B **3**, 869 (1991).

Downloaded 08 Nov 2012 to 194.81.223.66. Redistribution subject to AIP license or copyright; see http://pop.aip.org/about/rights_and_permissions